Electronic Supplementary Information (ESI†)
for

Ferrrocenyl-L-amino acid copper(II) complexes showing remarkable photo-induced anticancer activity in visible light

Tridib K. Goswami,[†] Sudarshan Gadadhar,[‡] Babu Balaji,[†] Bappaditya Gole,[†] Anjali A. Karande,*[,‡] and Akhil R. Chakravarty*[,†]

[†]*Department of Inorganic and Physical Chemistry, Indian Institute of Science, Bangalore 560012, India*

[‡]*Department of Biochemistry, Indian Institute of Science, Bangalore 560012, India*

Corresponding authors: Fax: 91-80-23600683. E-mail: arc@ipc.iisc.ernet.in (ARC) &

anjali@biochem.iisc.ernet.in (AAK)

Experimental Section

DNA binding methods. Calf thymus (ct) DNA binding experiments were performed in Tris-HCl and phosphate buffers at an ambient temperature. The DNA was found to be free of protein impurity as evidenced from the ratio of the absorbance values of the DNA at 260 and 280 nm in Tris-HCl buffer as 1.9:1. Concentration of the ct-DNA (in base pairs) was determined by absorption spectroscopy using its molar absorption coefficient value of 6600 dm^3 mol^{-1} cm^{-1} at 260 nm wavelength.[S1]

In UV-visible absorption titration experiments, the complex solution (40 μmol) in 5 mmol Tris-HCl buffer containing 20% DMF (pH = 7.19) was titrated with 235 μmol DNA and the intensity of the band at ~375 nm was monitored for the complexes. Due correction was made for the absorption of DNA itself. The spectra were recorded after equilibration for 5 min allowing the complexes to bind to the DNA. The intrinsic equilibrium binding constant (K_b) and the fitting parameter (s) of the complexes to DNA were obtained by McGhee-von Hippel (MvH) method using the expression of Bard and co-workers by measuring the change of the absorption intensity of the spectral bands with increasing concentration of DNA by regression analysis using eq. (1)

$$(\varepsilon_a - \varepsilon_f)/(\varepsilon_b - \varepsilon_f) = (b - (b^2 - 2K_b^2C_t[DNA]_t/s)^{1/2})/2K_bC_t \qquad \ldots (1)$$

where $b = 1 + K_bC_t + K_b[DNA]_t/2s$, ε_a is the extinction coefficient observed for the absorption band at a given DNA concentration, ε_f is the extinction coefficient of the complex free in solution, ε_b is the extinction coefficient of the complex when fully bound to DNA, K_b is the equilibrium binding constant, C_t is the total metal complex concentration, $[DNA]_t$ is the DNA concentration in nucleotides and s as the fitting parameter giving an estimate of the binding site size in base pairs.[S2,S3] The non-linear least-squares analysis was done using Origin Lab, version 6.1.

DNA thermal denaturation studies were carried out by monitoring the absorption intensity of the ct-DNA (200 μmol) at 260 nm varying the temperature from 40 °C to 90 °C at a rate of 0.5 °C per minute, both in the absence and in the presence of the complexes (20 μmol) in 5 mM phosphate buffer (pH 6.8). The experiments were done using a complex to DNA molar ratio of 2:7 and the measurements were made using a Cary 300 bio UV-Visible spectrometer with Cary temperature controller on increasing the temperature of the solution by 0.5 °C min^{-1}. Viscometric titration experiments were performed using Schott Gerate AVS310 Automated Viscometer that was thermostated at 37.0(±0.1) °C in a constant temperature bath. The concentration of ct-DNA was 160 μmol. The flow time was measured with an automated timer. The data were presented by plotting relative specific viscosity of DNA, $(\eta/\eta_0)^{1/3}$ vs. [complex]/[DNA], where η is the viscosity of DNA in the presence of the complex and η_0 is the viscosity of DNA alone in 5 mmol Tris-HCl buffer medium. The viscosity values were calculated from the observed flow time of DNA containing solutions (t) duly corrected for that of the buffer alone (t_0), $\eta = (t - t_0)/t_0$.[S4]

DNA cleavage experiments. The cleavage of supercoiled pUC19 DNA (30 μmol, 0.2 μg, 2686 base-pairs) was studied by agarose gel electrophoresis using the metal complexes in a 50 mmol tris(hydroxymethyl)methane-HCl (Tris-HCl) buffer (pH 7.16) containing 50 mmol NaCl. For photo-induced DNA cleavage studies, the reactions were carried out in visible light of 454, 568 and 647 nm wavelengths using a Spectra Physics Water-Cooled Mixed-Gas Ion Laser Stabilite® 2018-RM (continuous-wave (CW) beam diameter at $1/e^2 = 1.8$ mm ± 10% and beam divergence with full angle = 0.7 mrad ± 10%). The laser beam power at the sample position (5 cm from the aperture with a solution path length of 5 mm) was 50 mW, measured using Spectra Physics CW Laser Power Meter (Model 407A). After light exposure, each sample was incubated for 1.0 h at 37 °C and analyzed for the photo-cleaved products using agarose gel electrophoresis. The mechanistic studies were carried out using different additives for quenching singlet oxygen (NaN_3, 1 mmol; TEMP, 1.0 mmol; L-histidine, 1.0 mmol) and scavenging hydroxyl radicals (DMSO, 4 μl; KI, 1.0 mmol; catalase, 4 units) prior to the addition of the complex. Superoxide dismutase was used as a scavenger of $O_2^{\bullet-}$ radicals. The samples after incubation in a dark chamber were added to the loading buffer containing 0.25% bromophenol blue, 0.25% xylene cyanol, 30% glycerol (3 μl) and the solution was finally loaded on 1% agarose gel containing 1.0 μg ml^{-1} ethidium bromide. Electrophoresis was carried out in a dark chamber for 2.0 h at 60 V in TAE (Tris-acetate EDTA) buffer. Bands were visualized by UV light and photographed. The extent of DNA cleavage was calculated from the intensities of the bands using UVITEC Gel Documentation System. Due corrections were done for the low level of NC form present in the original supercoiled (SC) DNA sample and for the low affinity of EB binding to SC compared to NC form of DNA.[S5] The concentrations of the complexes and additives corresponded to that in the 20 μl final volume of the sample using Tris buffer. The estimated error in measuring the band intensities ranged within 3-5%.

References

S1. M. E. Reichman, S. A. Rice, C. A. Thomas and P. Doty, *J. Am. Chem. Soc.*, 1954, **76**, 3047-3053.

S2. J. D. McGhee and P. H. Von Hippel, *J. Mol. Biol.*, 1974, **86**, 469-489.

S3. M. T. Carter, M. Rodriguez and A. J. Bard, *J. Am. Chem. Soc.*, 1989, **111**, 8901-8911.

S4. G. Cohen and H. Eisenberg, *Biopolymers*, 1969, **8**, 45-55.

S5. J. Bernadou, G. Pratviel, F. Bennis, M. Girardet and B. Meunier, *Biochemistry*, 1989, **28**, 7268-7275.

Table S1 Selected bond distances (Å) and bond angles (°) of [Cu(Fc-Tyr)(aip)](ClO_4) (**1**), [Cu(Fc-Trp)(aip)](ClO_4) (**2**) and [Cu(Fc-Met)(aip)](ClO_4) (**3**) obtained from DFT calculations

	[Cu(Fc-Tyr)(aip)] (ClO_4) (**1**)	[Cu(Fc-Trp)(aip)] (ClO_4) (**2**)	[Cu(Fc-Met)(aip)] (ClO_4) (**3**)
Cu(1)-O(1)	1.93	1.93	1.95
Cu(1)-N(1)	2.06	2.06	2.08
Cu(1)-N(2)	2.06	2.06	2.08
Cu(1)-N(3)	2.01	2.01	2.02
Cu(1)-S(1)	-	-	2.84
O(1)-Cu(1)-N(1)	81.66	81.74	82.08
O(1)-Cu(1)-N(3)	90.11	90.36	88.92
N(1)-Cu(1)-N(2)	105.92	105.94	106.54
N(2)-Cu(1)-N(3)	82.20	82.08	81.58
O(1)-Cu(1)-N(2)	171.62	172.40	169.79
N(1)-Cu(1)-N(3)	171.72	172.09	166.18
O(1)-Cu(1)-S(1)	-	-	96.93
N(1)-Cu(1)-S(1)	-	-	84.68
N(2)-Cu(1)-S(1)	-	-	89.44
N(3)-Cu(1)-S(1)	-	-	106.91

Table S2 Selected bond distances (Å) and bond angles (°) of [Cu(Fc-Tyr)(pyip)](ClO_4) (**4**), [Cu(Fc-Trp)(pyip)](ClO_4) (**5**) and [Cu(Fc-Met)(pyip)](ClO_4) (**6**) obtained from DFT calculations.

	[Cu(Fc-Tyr)(pyip)] (ClO_4) (**4**)	[Cu(Fc-Trp)(pyip)] (ClO_4) (**5**)	[Cu(Fc-Met)(pyip)] (ClO_4) (**6**)
Cu(1)-O(1)	1.93	1.93	1.95
Cu(1)-N(1)	2.06	2.06	2.08
Cu(1)-N(2)	2.06	2.06	2.08
Cu(1)-N(3)	2.01	2.00	2.02
Cu(1)-S(1)	-	-	2.84
O(1)-Cu(1)-N(1)	81.97	81.89	82.02
O(1)-Cu(1)-N(3)	90.02	90.05	89.00
N(1)-Cu(1)-N(2)	105.83	105.94	106.46
N(2)-Cu(1)-N(3)	82.29	82.17	81.65
O(1)-Cu(1)-N(2)	171.58	172.14	169.98
N(1)-Cu(1)-N(3)	171.73	171.01	166.15
O(1)-Cu(1)-S(1)	-	-	97.77
N(1)-Cu(1)-S(1)	-	-	83.93
N(2)-Cu(1)-S(1)	-	-	88.58
N(3)-Cu(1)-S(1)	-	-	107.84

Table S3 Energies of highest occupied molecular orbital (HOMO) and lowest unoccupied molecular orbital (LUMO) of the complexes **1-6** obtained from DFT calculations

Complex	Energy (eV)		HOMO-LUMO energy difference (eV)
	HOMO	LUMO	
1	-7.4014	-5.3987	2.0027
2	-7.4967	-5.3470	2.1497
3	-7.5266	-5.2953	2.2313
4	-7.3903	-5.3527	2.0376
5	-7.4994	-5.2898	2.2096
6	-7.5340	-5.2267	2.3073

Table S4 IC_{50} values of the ligands and copper(II) nitrate in HeLa and MCF-7 cancer cells

Compound	HeLa		MCF-7	
	IC_{50} (μmol) dark[a]	IC_{50} (μmol) visible light[b]	IC_{50} (μmol) dark[a]	IC_{50} (μmol) visible light[b]
Fc-TyrH[c]	>200	>200	>200	>200
Fc-TrpH[d]	>200	>200	>200	>200
Fc-MetH[e]	>200	>200	>200	>200
$Cu(NO_3)_2·3H_2O$[e]	>200	169.0 ± 4.0	-	-

[a] The IC_{50} values correspond to 24 h incubation in dark. [b] The IC_{50} values correspond to 4 h incubation in dark followed by photo-exposure to visible light (400-700 nm, 10 J cm^{-2}). [c] T. K. Goswami, S. Gadadhar, A. A. Karande and A. R. Chakravarty, *Polyhedron*, 2013, **52**, 1287-1298. [d] T. K. Goswami, B. V. S. K. Chakravarthi, M. Roy, A. A. Karande and A. R. Chakravarty, *Inorg. Chem.*, 2011, **50**, 8452-8464. [e] T. K. Goswami, S. Gadadhar, M. Roy, M. Nethaji, A. A. Karande and A. R. Chakravarty, *Organometallics*, 2012, **31**, 3010-3021.

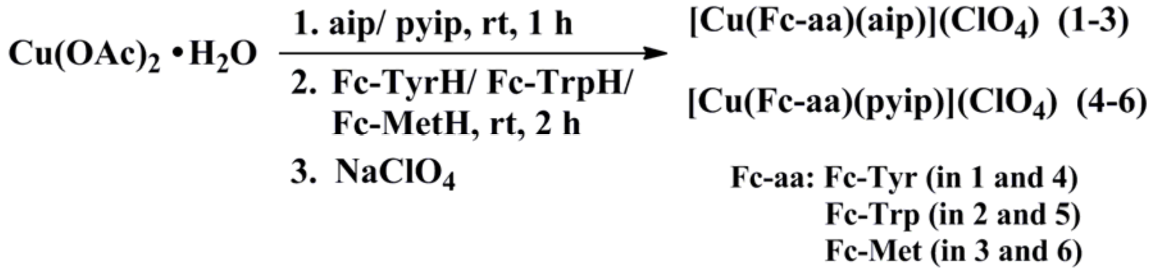

Scheme S1. Preparative scheme used for the complexes **1-6**, where aip or pyip is 2-(9-anthryl)-1*H*-imidazo[4,5-*f*][1,10]phenanthroline or 2-(1-pyrenyl)-1*H*-imidazo[4,5-*f*][1,10]phenanthroline; Fc-TyrH is ferrocenylmethyl-L-tyrosine and Fc-MetH is ferrocenylmethyl-L-methionine.

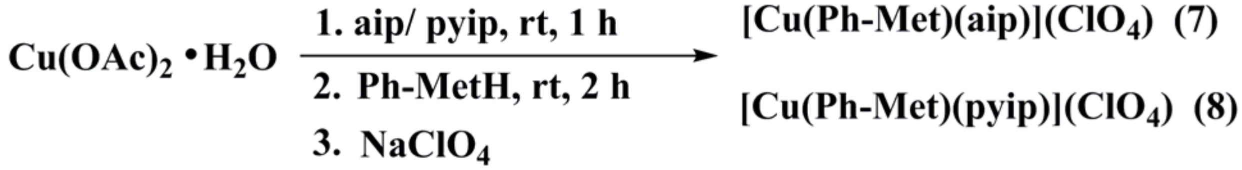

Scheme S2. Preparative scheme used for the complexes **7** and **8**, where aip or pyip is 2-(9-anthryl)-1*H*-imidazo[4,5-*f*][1,10]phenanthroline or 2-(1-pyrenyl)-1*H*-imidazo[4,5-*f*][1,10]phenanthroline and Ph-MetH is phenylmethyl-L-methionine.

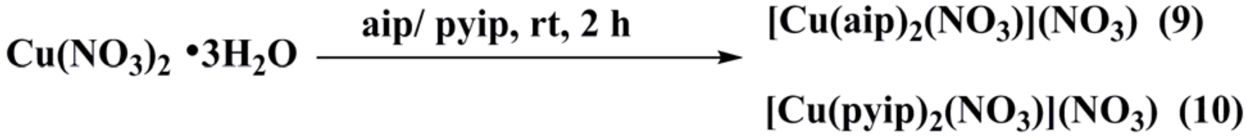

Scheme S3. Preparative scheme used for the complexes **9** and **10**, where aip or pyip is 2-(9-anthryl)-1*H*-imidazo[4,5-*f*][1,10]phenanthroline or 2-(1-pyrenyl)-1*H*-imidazo[4,5-*f*][1,10]phenanthroline.

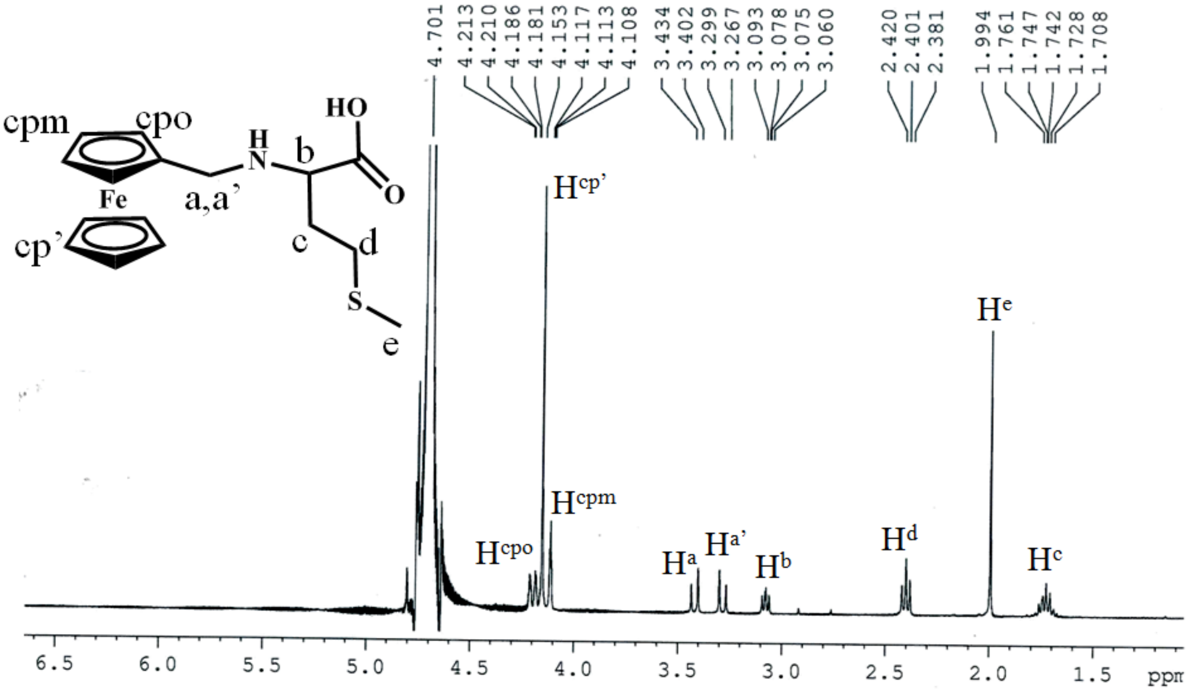

Figure S1. The ^{1}H-NMR spectrum of Fc-MetH in D_2O.

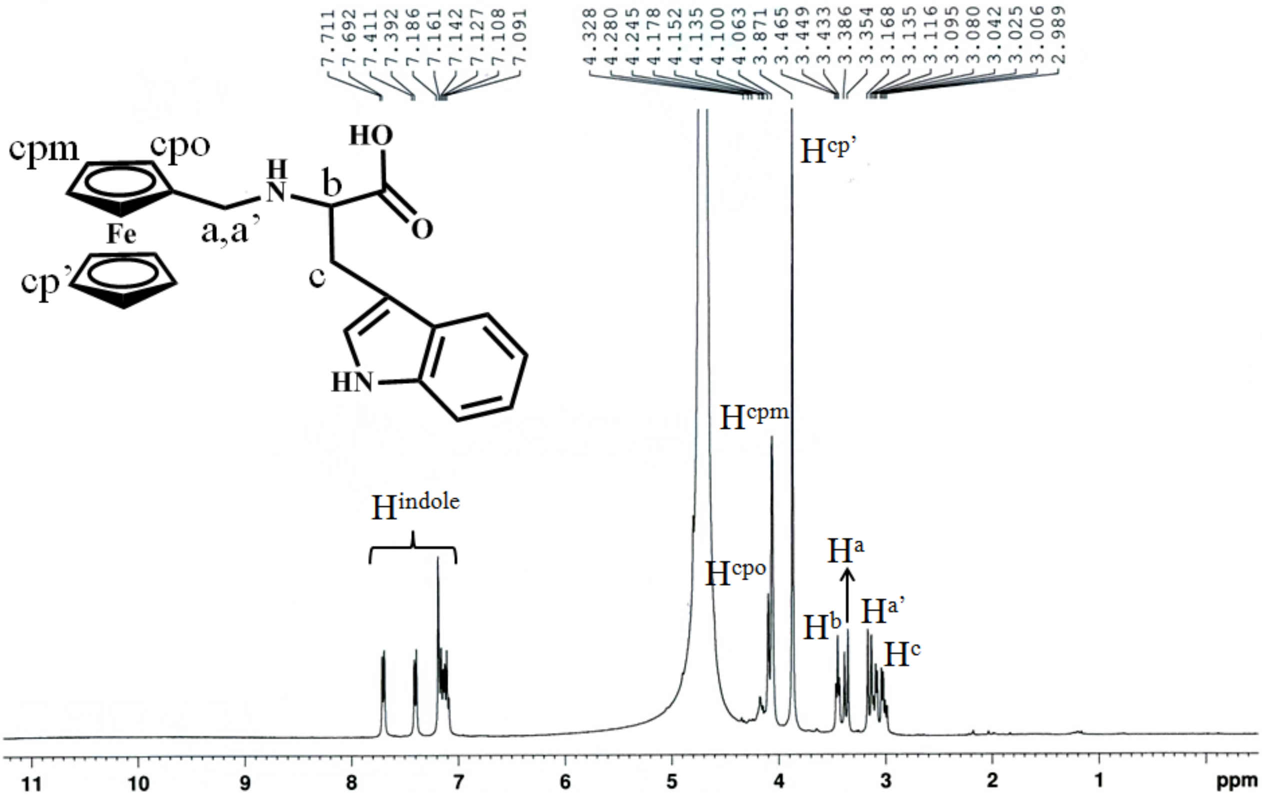

Figure S2. The ^{1}H-NMR spectrum of Fc-TrpH in D_2O.

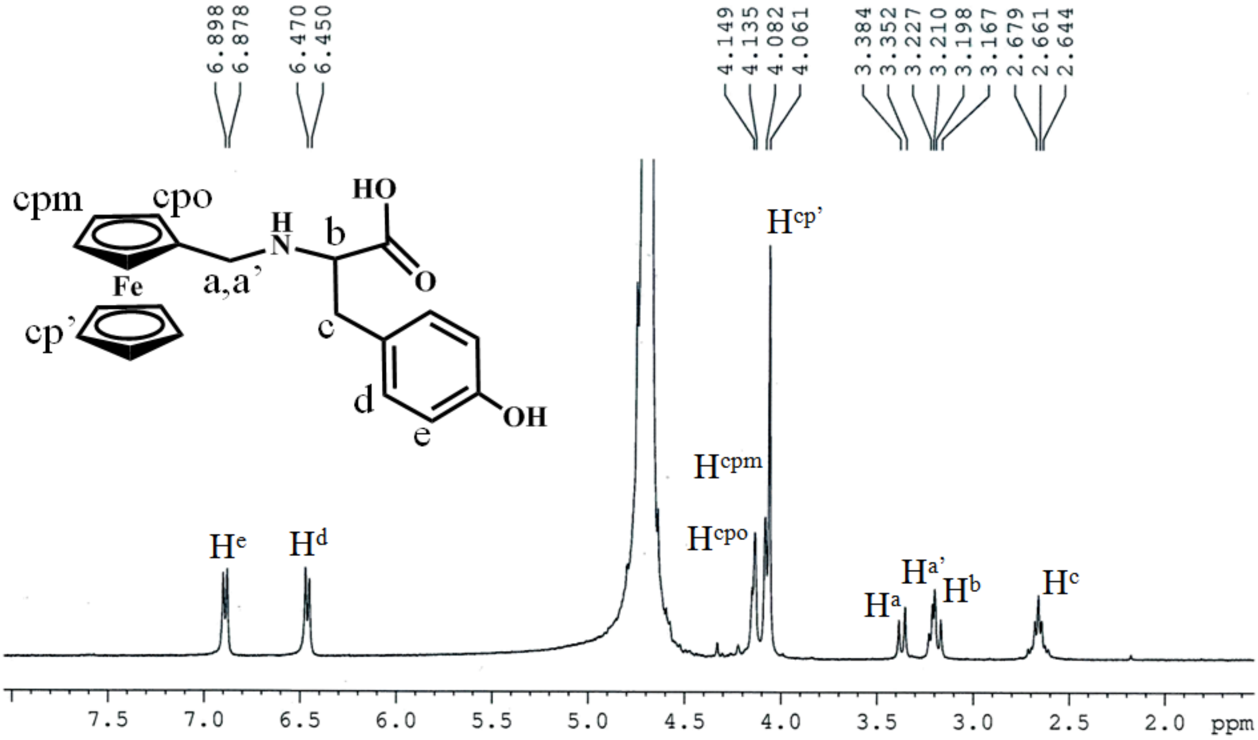

Figure S3. The ^{1}H-NMR spectrum of Fc-TyrH in D_2O.

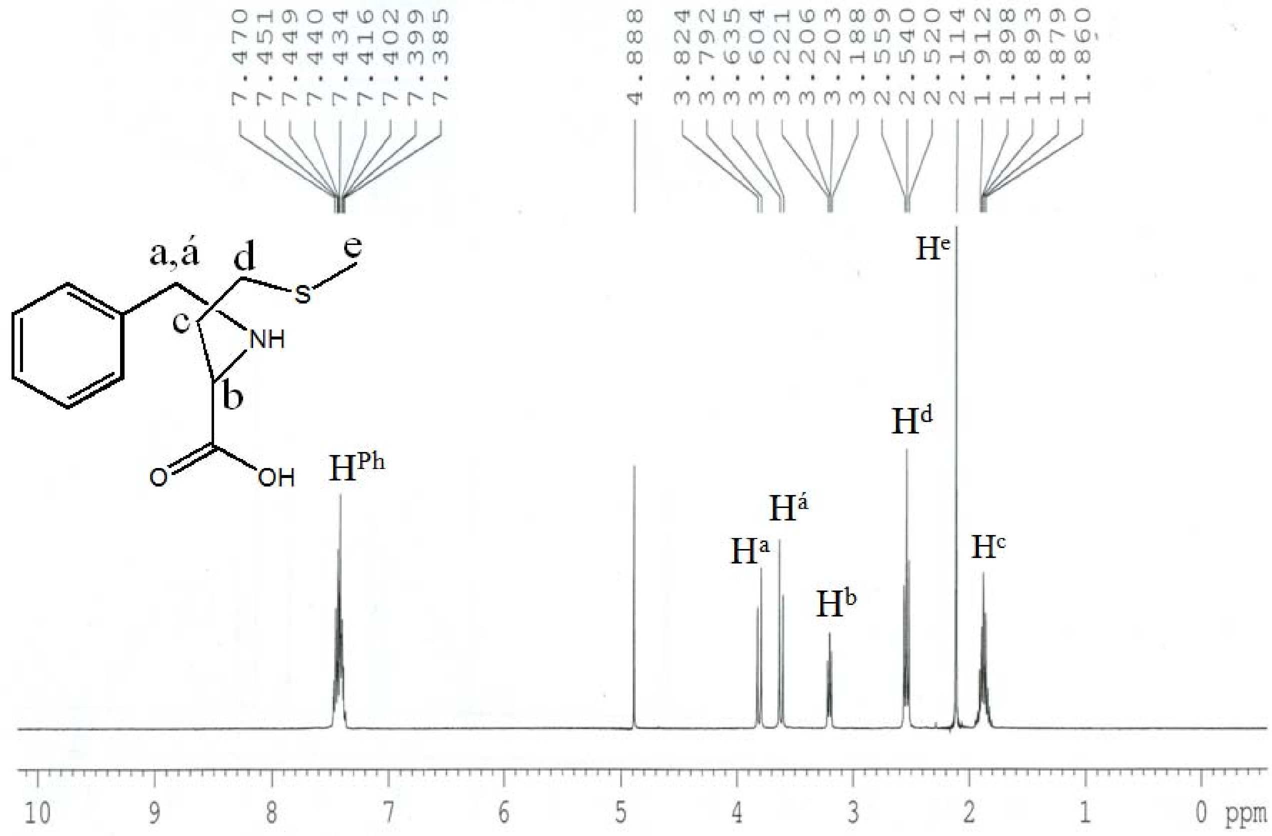

Figure S4. The ^{1}H-NMR spectrum of Ph-MetH in D_2O.

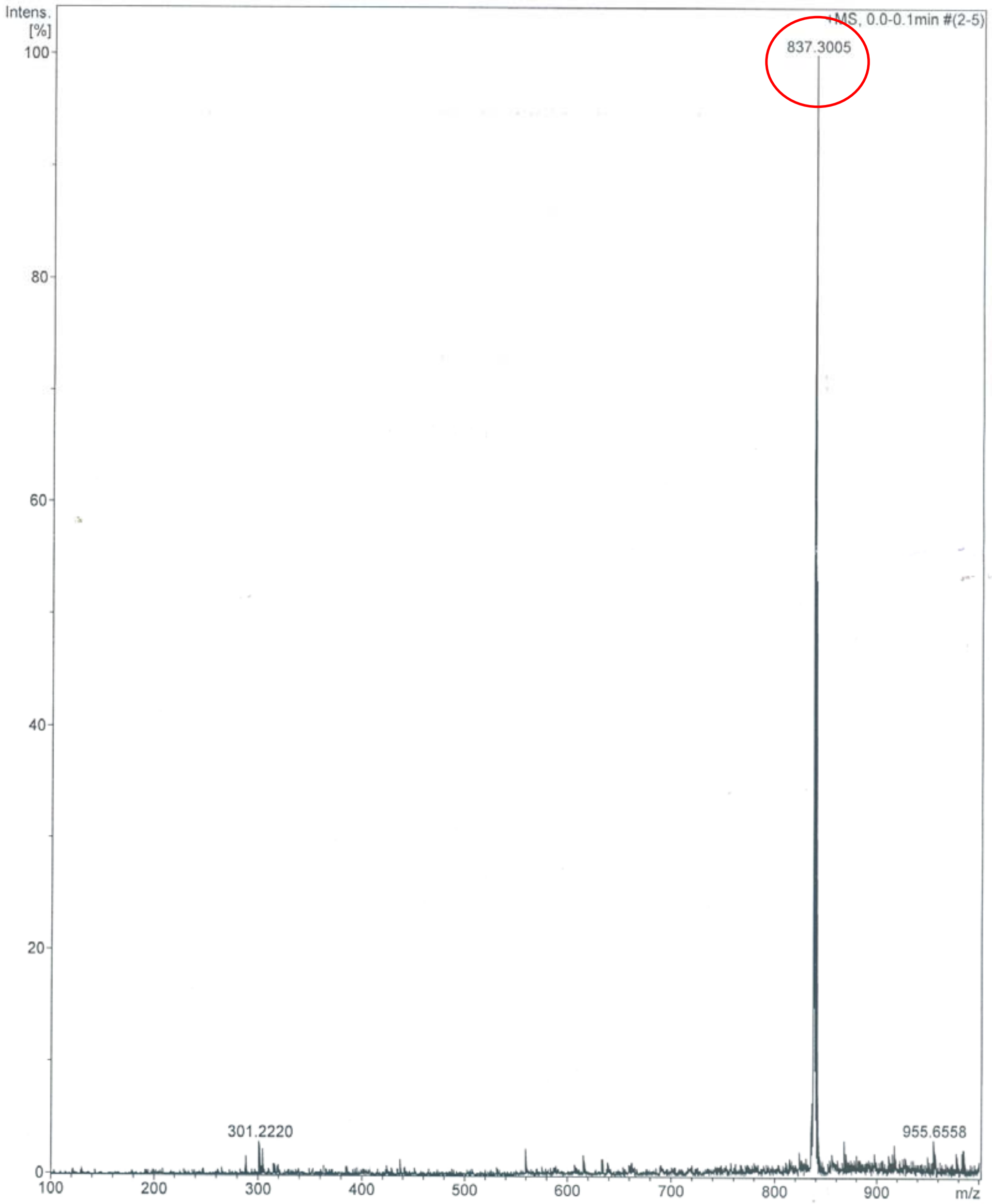

Fig. S5. ESI-MS spectrum of [Cu(Fc-Tyr)(aip)](ClO_4) (**1**) in MeOH showing the prominent [M-(ClO_4^-)]$^+$ peak.

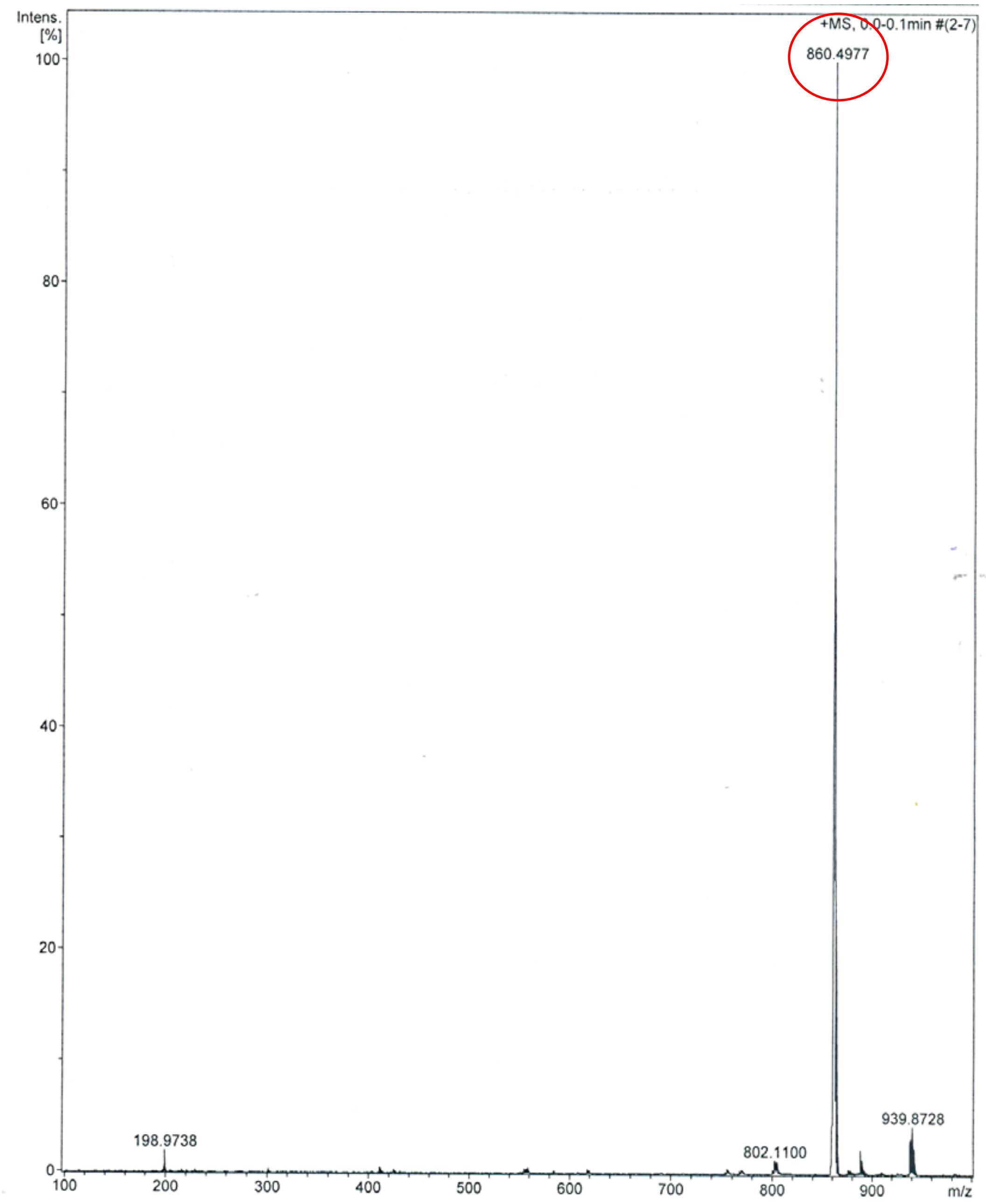

Fig. S6. ESI-MS spectrum of [Cu(Fc-Trp)(aip)](ClO_4) (**2**) in MeOH showing the prominent [M-(ClO_4^-)]$^+$ peak.

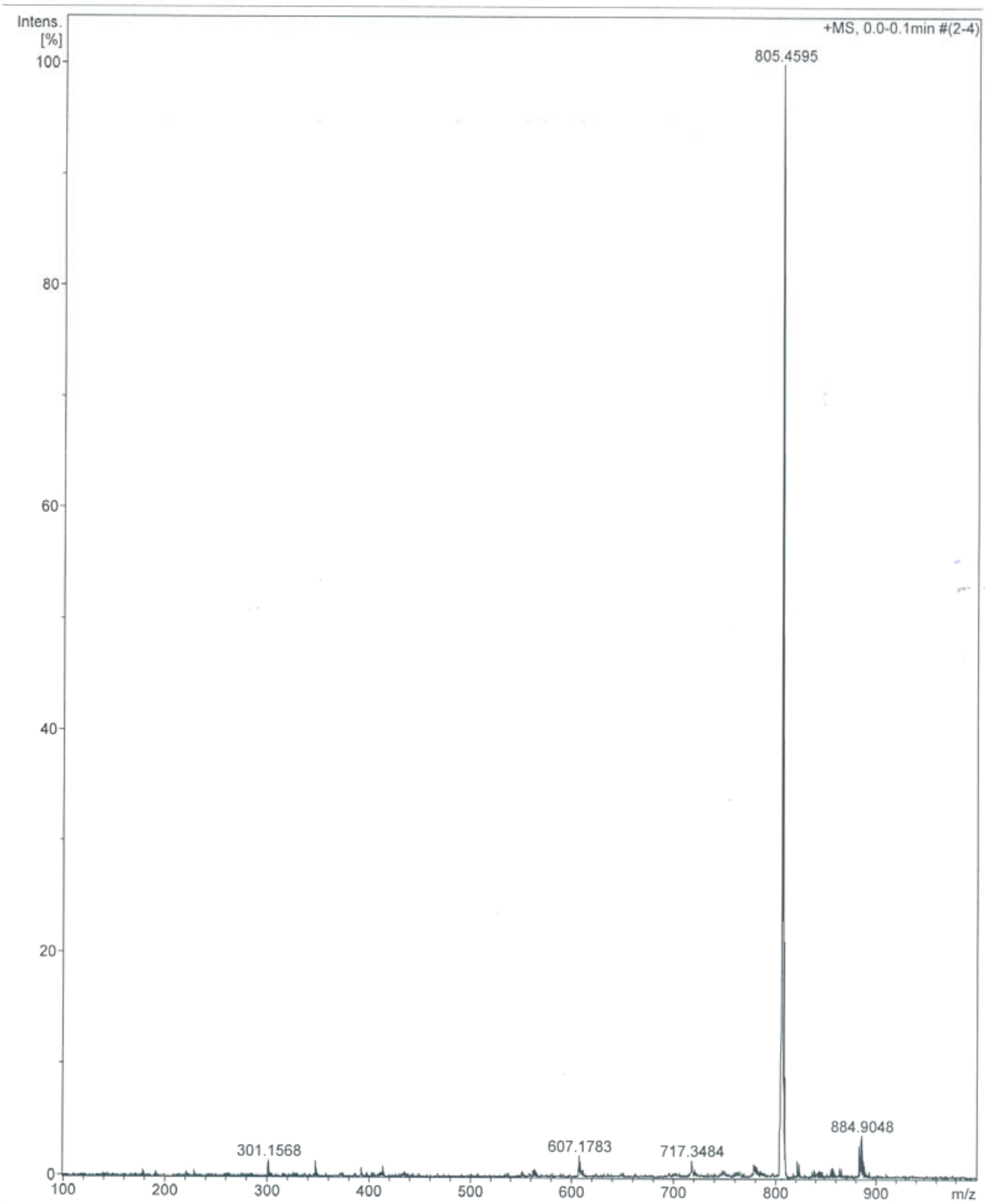

Fig. S7. ESI-MS spectrum of [Cu(Fc-Met)(aip)](ClO_4) (**3**) in MeOH showing the prominent [M-(ClO_4^-)]$^+$ peak.

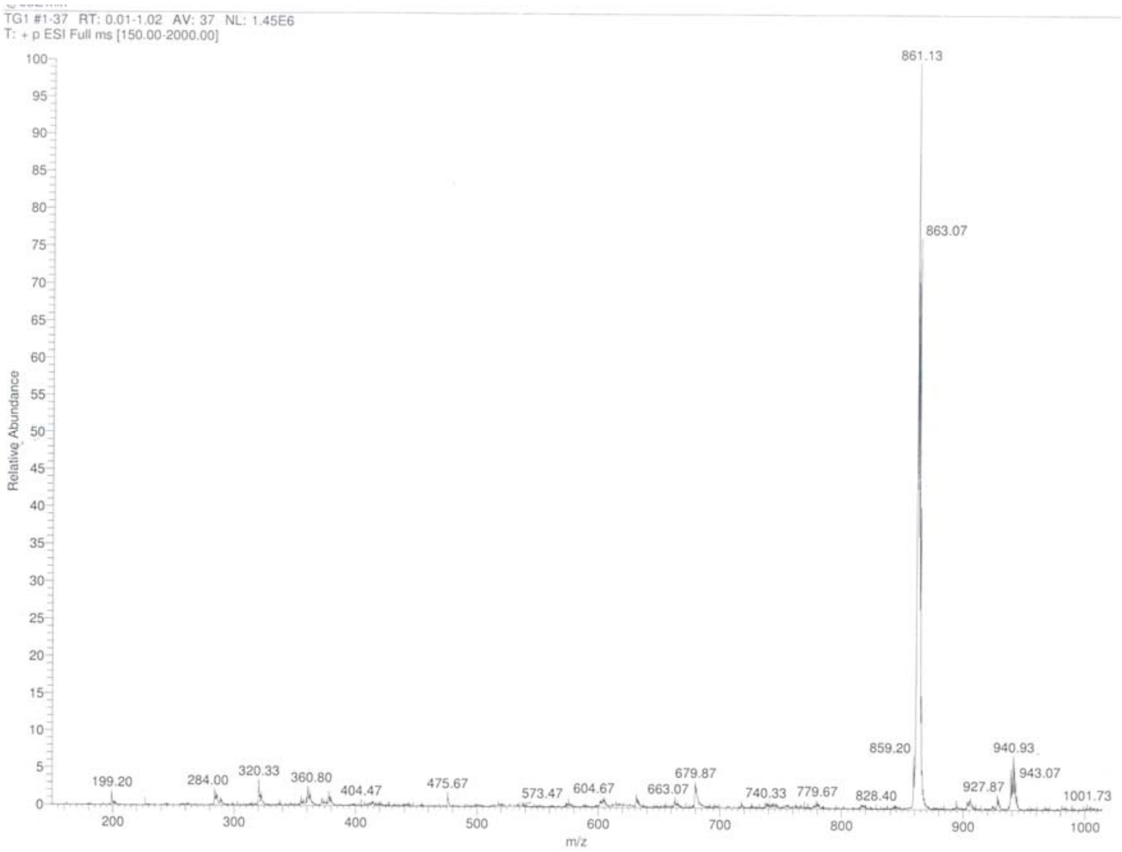

Fig. S8. ESI-MS spectrum of [Cu(Fc-Tyr)(pip)](ClO$_4$) (**4**) in MeOH showing the prominent [M-(ClO$_4^-$)]$^+$ peaks with well resolved copper isotropic distribution.

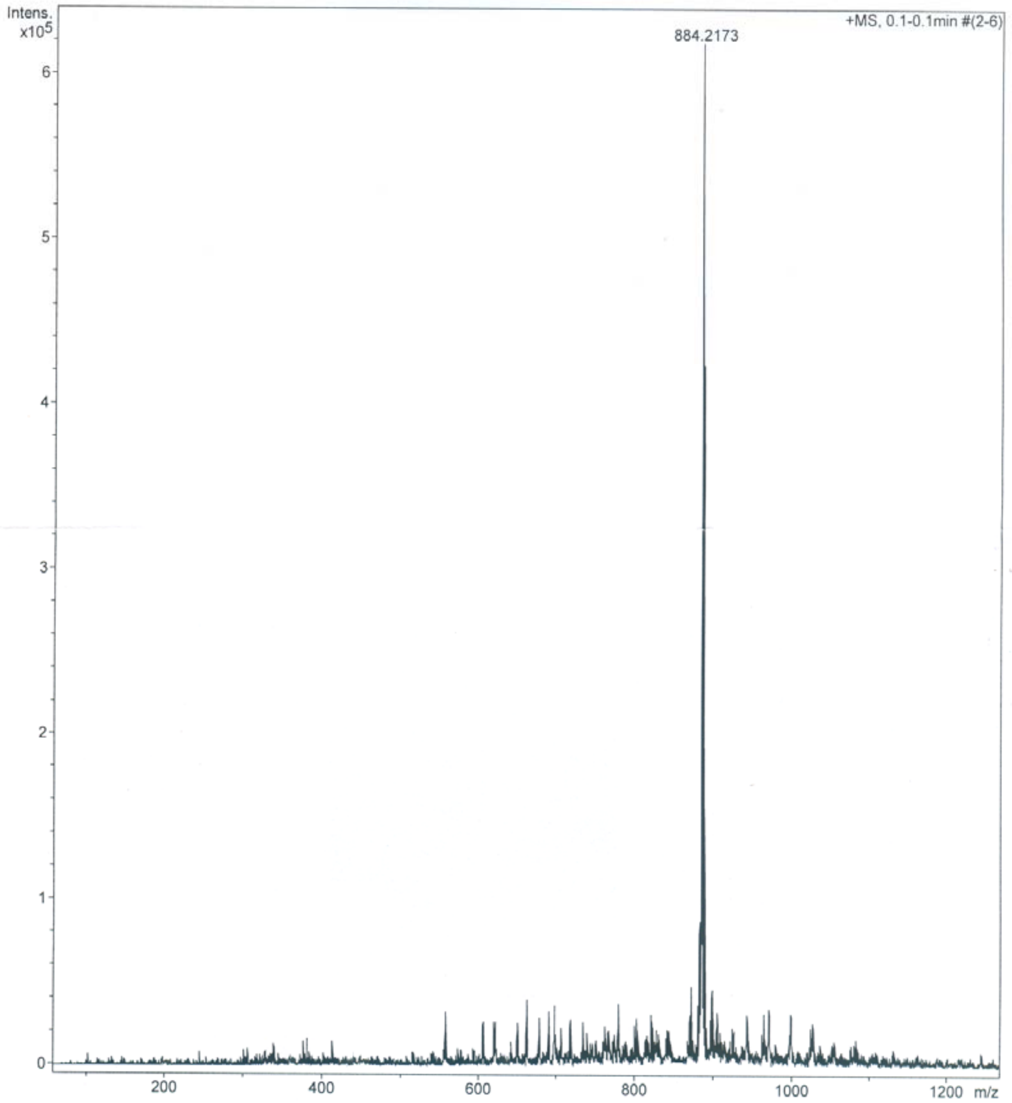

Fig. S9. ESI-MS spectrum of [Cu(Fc-Trp)(pip)](ClO_4) (**5**) in MeOH showing the prominent [M-(ClO_4^-)]$^+$ peak.

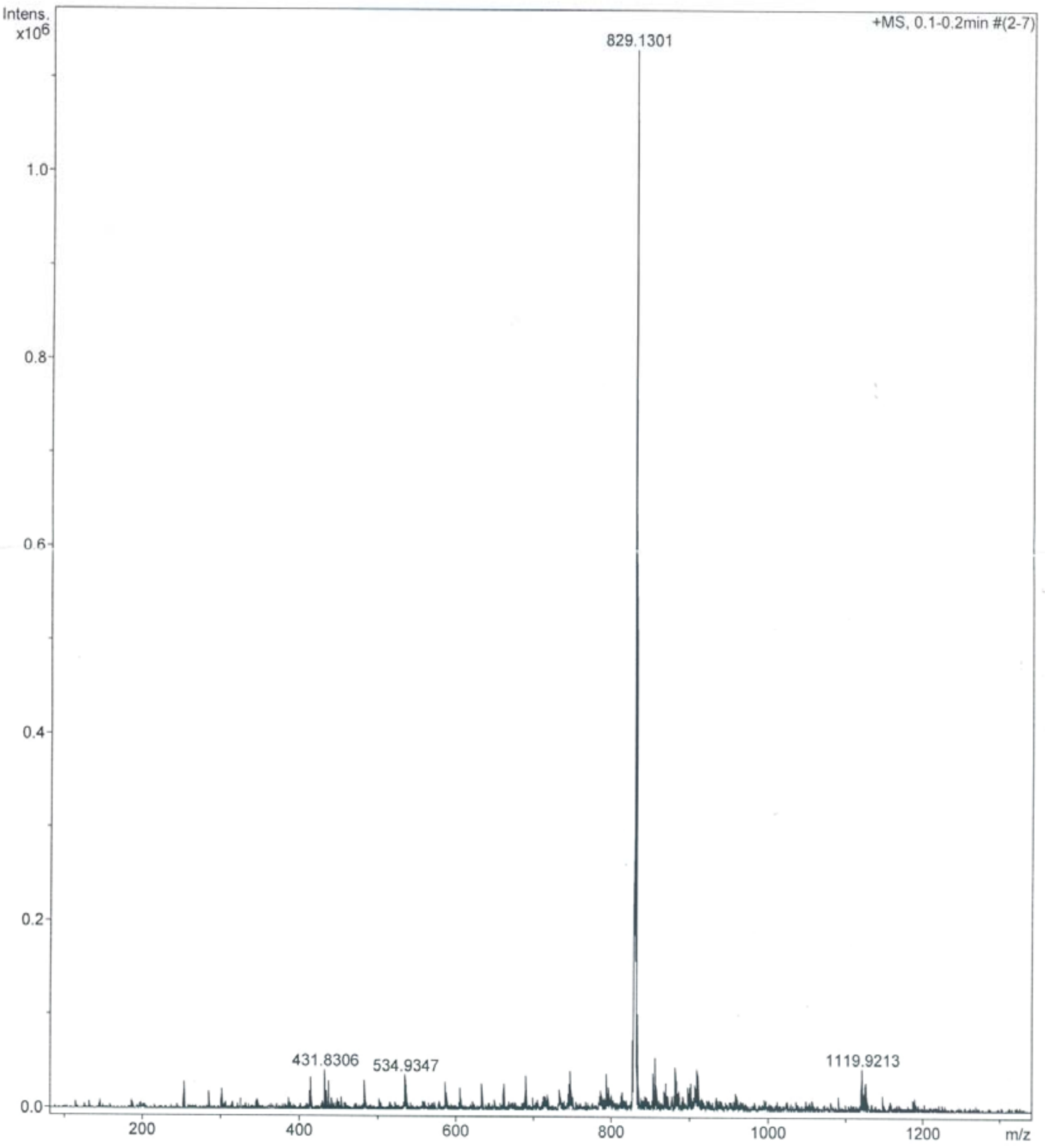

Fig. S10. ESI-MS spectrum of [Cu(Fc-Met)(pip)](ClO_4) (**6**) in MeOH showing the prominent [M-(ClO_4^-)]$^+$ peak.

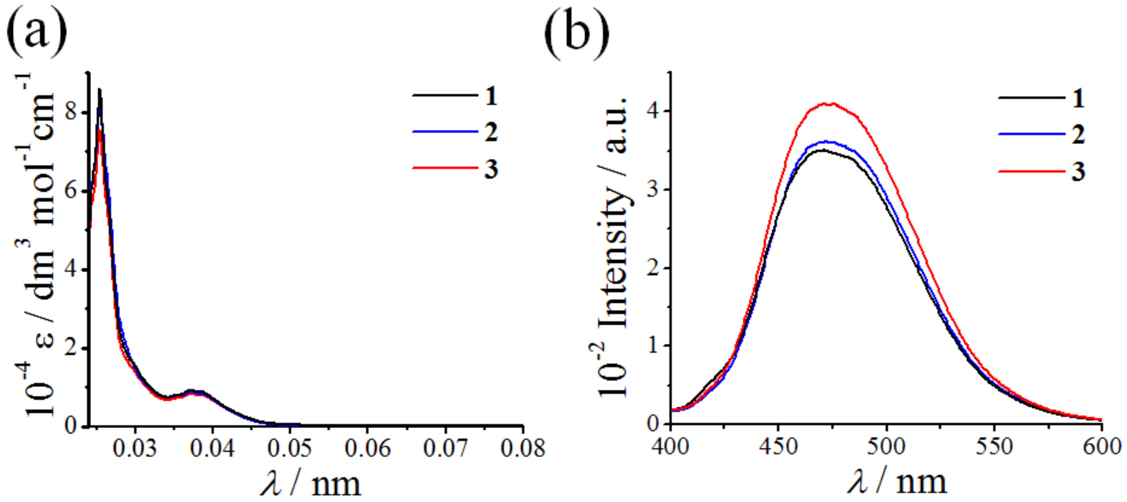

Fig. S11 (a) The electronic absorption spectra of **1-3** in DMF-Tris-HCl buffer (1:1 v/v, pH 7.2). (b) The emission spectra of the complexes in DMF (λ_{ex} = 370 nm).

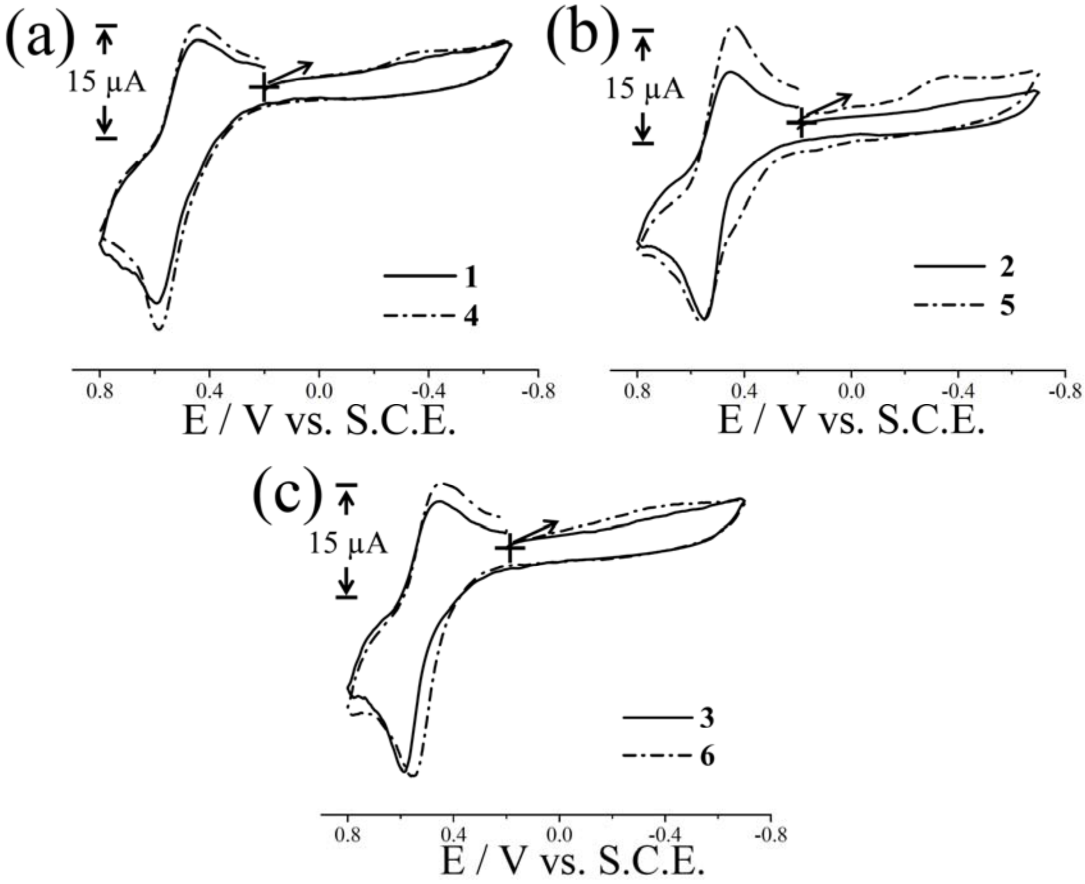

Fig. S12. Cyclic voltammetric responses of the complexes **1-6** in DMF-0.1 mol TBAP at a scan rate of 50 mV s^{-1}.

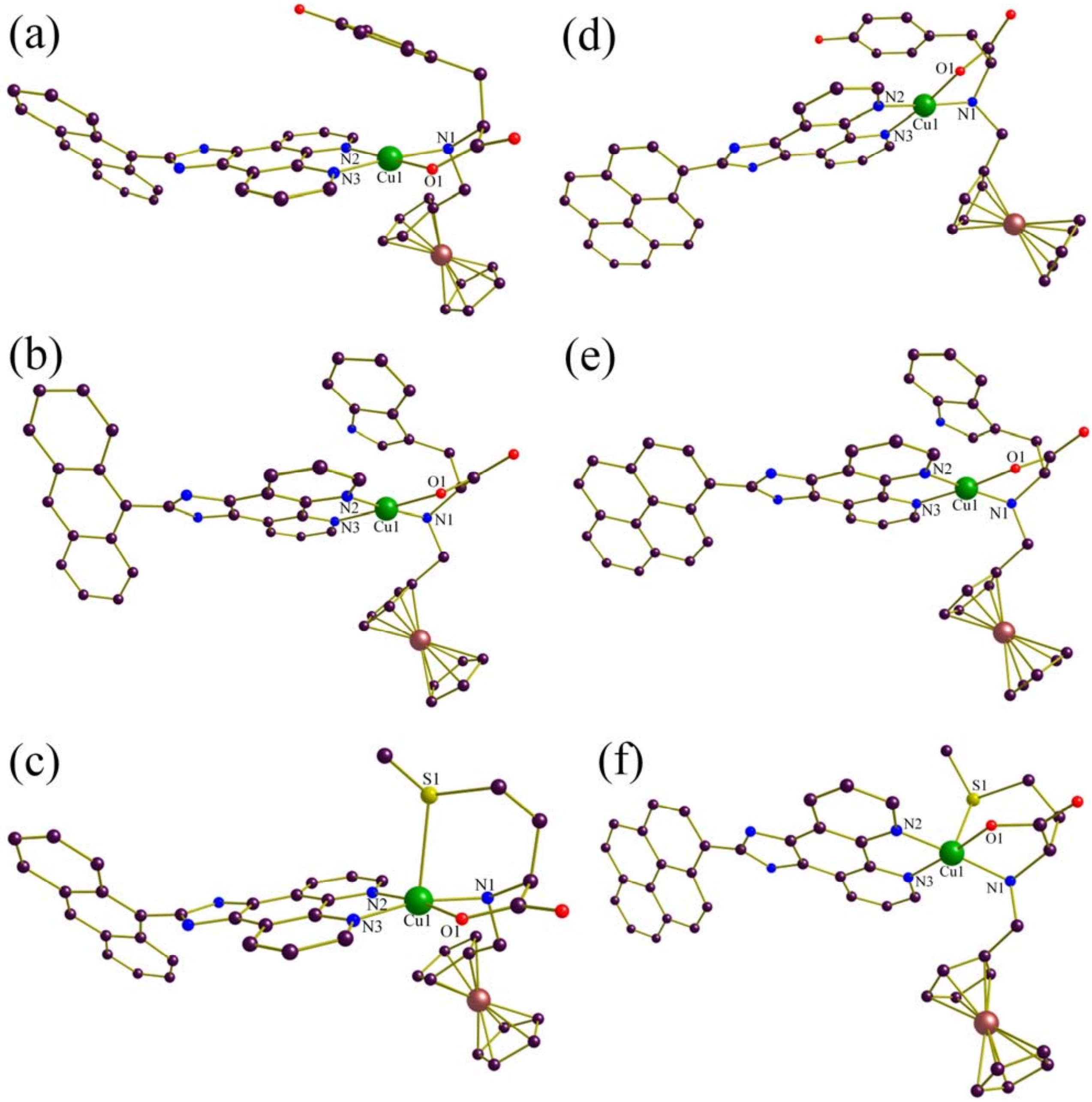

Fig. S13. View of the optimized structures of the complexes **1-6** (a-f) obtained by the DFT method. The hydrogen atoms are removed for clarity [Color code: purple, C; red, O; blue, N; wine red, Fe; green, Cu]. The axial sites of the copper(II) are sterically blocked by the pendant groups of ferrocenylmethyl-L-amino acid ligands in the structures shown in (a), (b), (d), (e). One axial site is blocked and the other is ligated by a thiomethyl group in (c) and (f).

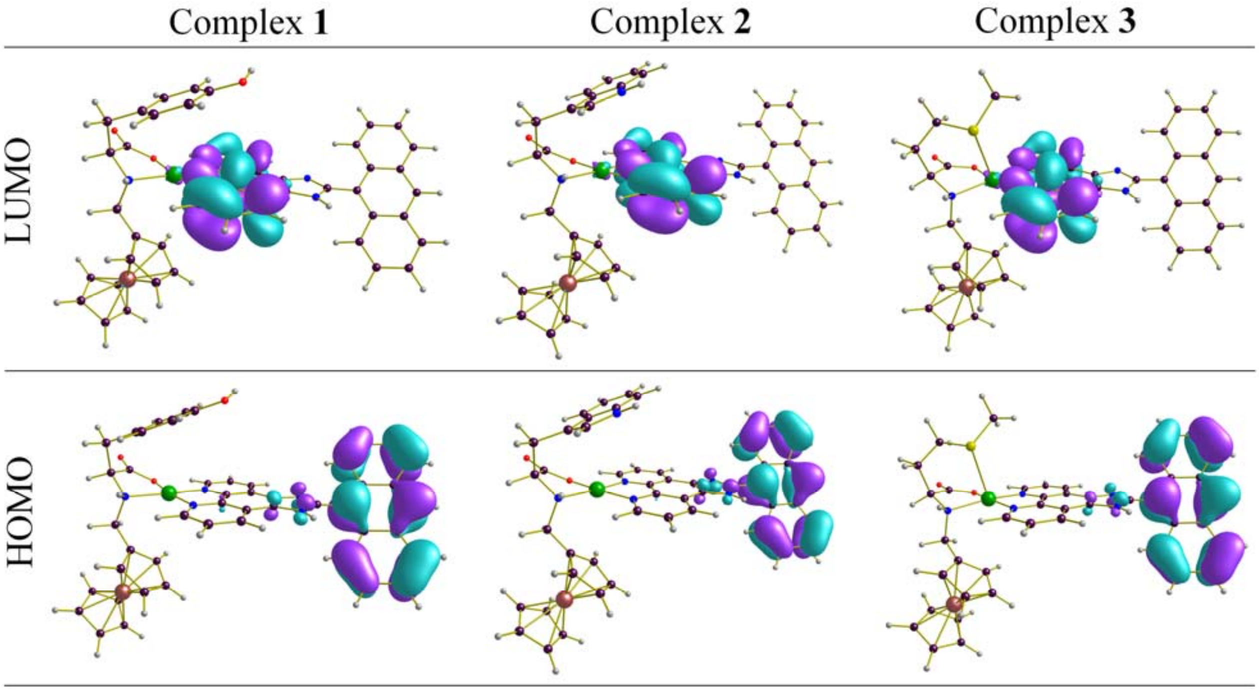

Fig. S14. Frontier orbitals of the complexes **1**-**3** with contour value of 0.03 a.u.

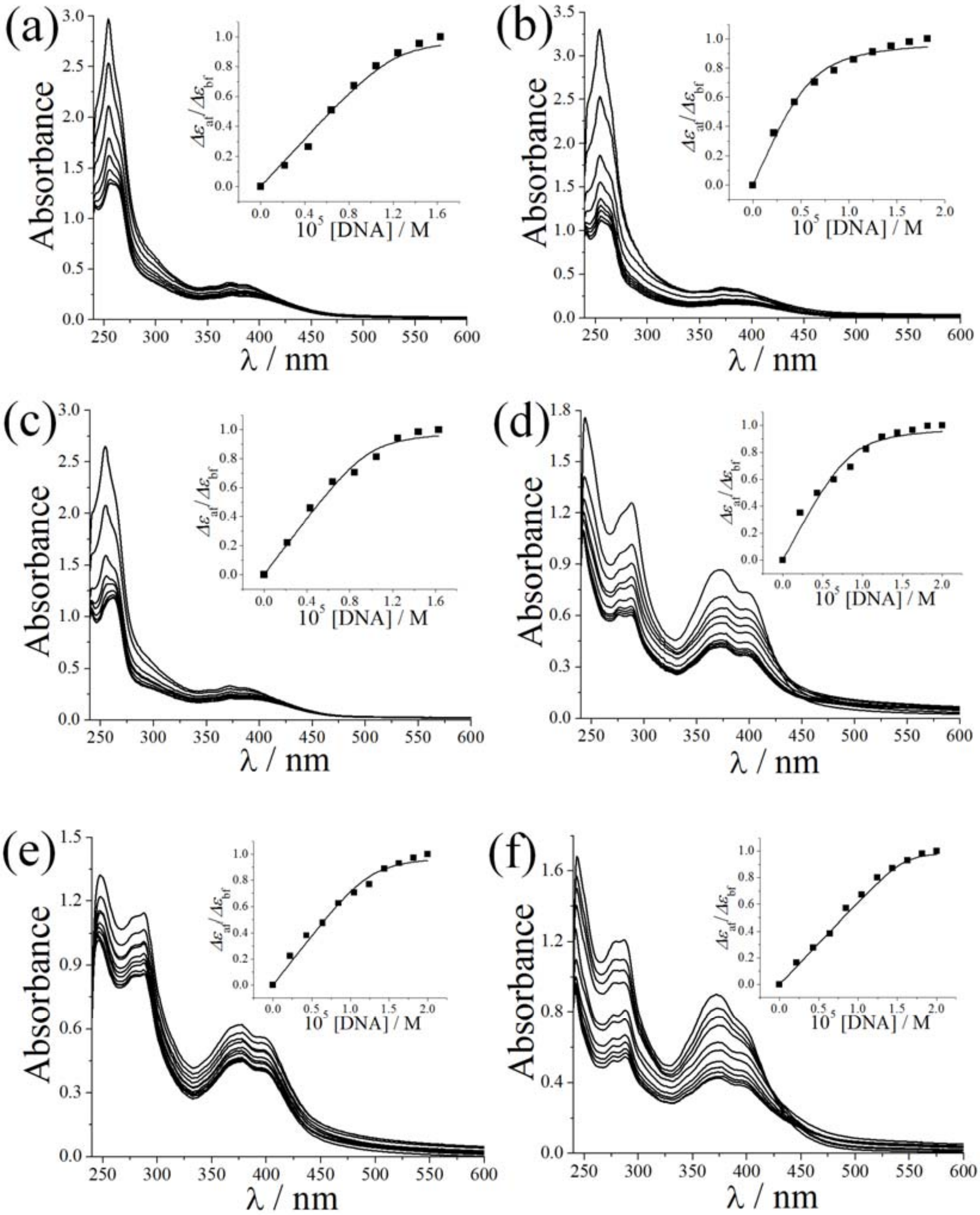

Fig. S15. Absorption spectral traces of the complexes **1-6** [(a)-(f)] in 5 mmol Tris-HCl buffer (pH 7.2) on increasing the quantity of calf thymus DNA. The inset shows the least-squares fits of $\Delta\varepsilon_{af}/\Delta\varepsilon_{bf}$ vs. [DNA] for the complexes.

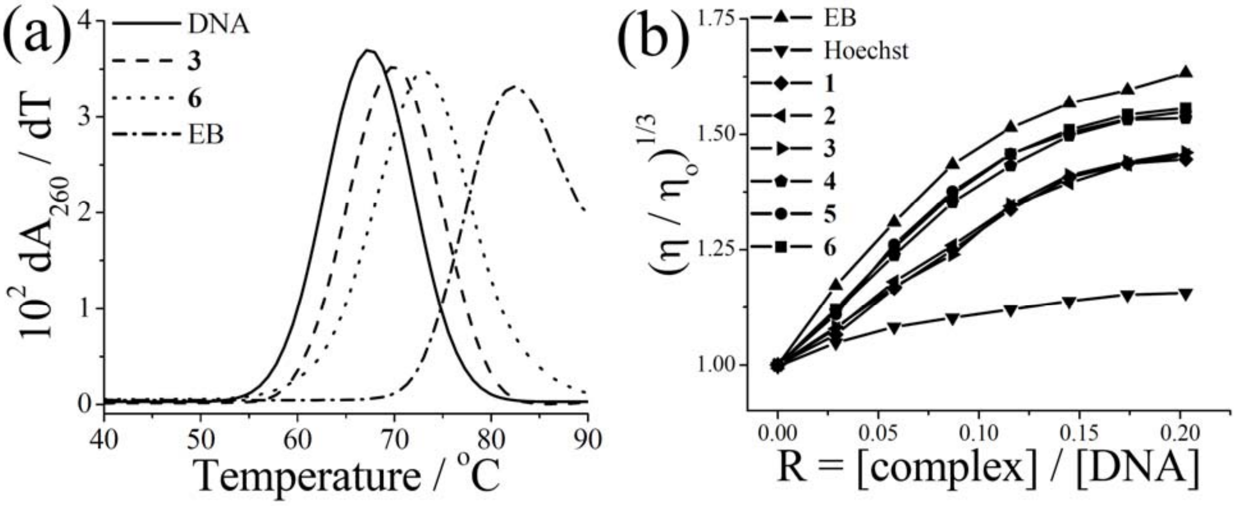

Fig. S16. (a) DNA melting temperature plot using ct-DNA (200 μmol NP) in the absence and presence of 20 μmol ethidium bromide (EB) and complexes **3** and **6** in 5 mM phosphate buffer (pH = 6.8). (b) The effect of increasing concentration of EB, Hoechst dye and the complexes **1**-**6** on the relative viscosity of ct-DNA at 37.0(±0.1) °C in 5 mmol Tris-HCl buffer (pH = 7.2, [ct-DNA] = 160 μmol).

Fig. S17. Gel electrophoresis diagram showing the chemical nuclease activity of the complexes **1-6** (5 µmol) and $[Cu(phen)_2(NO_3)](NO_3)$ (5 µmol) using SC pUC19 DNA (0.2 µg, 30 µmol b.p. (base pairs)) in the presence of 1.0 mmol glutathione (GSH) as a reducing (lanes 2-8) and 200 µmol H_2O_2 as an oxidizing agent (lanes 9-14) for an incubation time of 2 h: lane-1, DNA control; lane-2, DNA + **1**; lane-3, DNA + **2**; lane-4, DNA + **3**; lane-5, DNA + **4**; lane-6, DNA + **5**; lane-7, DNA + **6**; lane-8, DNA + $[Cu(phen)_2(NO_3)](NO_3)$ as a control complex; lane-9, DNA + **1**; lane-10, DNA + **2**; lane-11, DNA + **3**; lane-12, DNA + **4**; lane-13, DNA + **5**; lane-14, DNA + **6**.

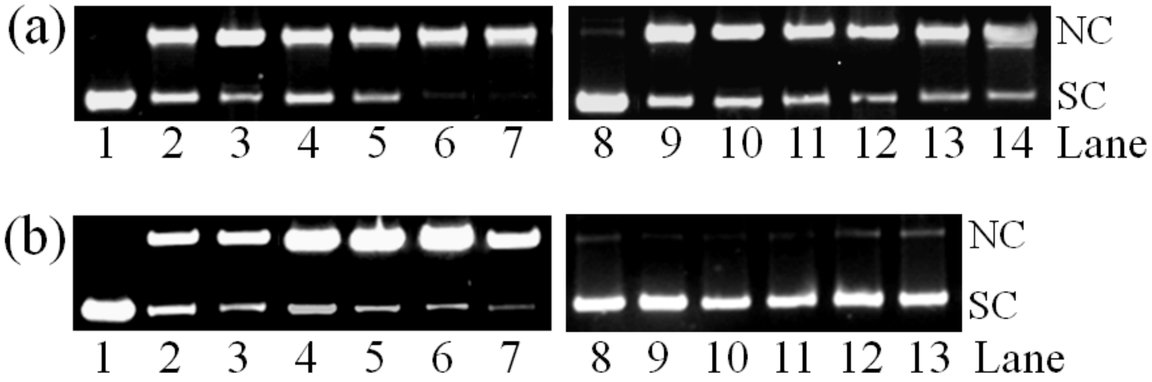

Fig. S18. Gel electrophoresis diagrams showing the photocleavage of SC pUC19 DNA (0.2 μg, 30 μmol b.p.) by the complexes **1-6** (10 μmol for 454 nm and 15 μmol for other wavelengths) on irradiation with light of various laser wavelengths (50 mW, exposure time: 2 h) [(a) 454 nm (lanes 1-7) and 568 nm (lanes 8-14), (b) 647 nm (lanes 1-7) and dark (lanes 8-13)]: (a) lane-1, DNA control (454 nm); lane-2, DNA + **1**; lane-3, DNA + **2**; lane-4, DNA + **3**; lane-5, DNA + **4**; lane-6, DNA + **5**; lane-7, DNA + **6**; lane-8, DNA control (568 nm); lane-9, DNA + **1**; lane-10, DNA + **2**; lane-11, DNA + **3**; lane-12, DNA + **4**; lane-13, DNA + **5**; lane-14, DNA + **6** and (b) lane-1, DNA control (647 nm); lane-2, DNA + **1**; lane-3, DNA + **2**; lane-4, DNA + **3**; lane-5, DNA + **4**; lane-6, DNA + **5**; lane-7, DNA + **6**; lane-8, DNA + **1** lane-9, DNA + **2**; lane-10, DNA + **3**; lane-11, DNA + **4**; lane-12, DNA + **5**; lane-13, DNA + **6**.

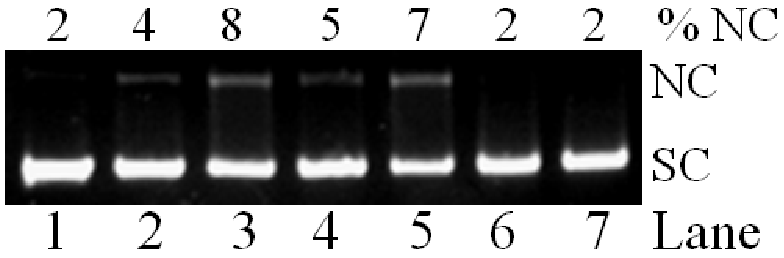

Fig. S19. Gel electrophoresis diagram showing the photocleavage of SC pUC19 DNA (0.2 μg, 30 μmol b.p.) by the ligands (15 μmol) on irradiation with 454 and 647 nm laser radiation (50 mW) for an exposure time of 2 h: lane-1, DNA control (454 nm); lane-2, DNA + aip ligand (454 nm); lane-3, DNA + pyip ligand (454 nm); lane-4, DNA + aip ligand (647 nm); lane-5, DNA + pyip ligand (647 nm); lane-6, DNA + aip ligand (dark); lane-7, DNA + pyip ligand (dark).

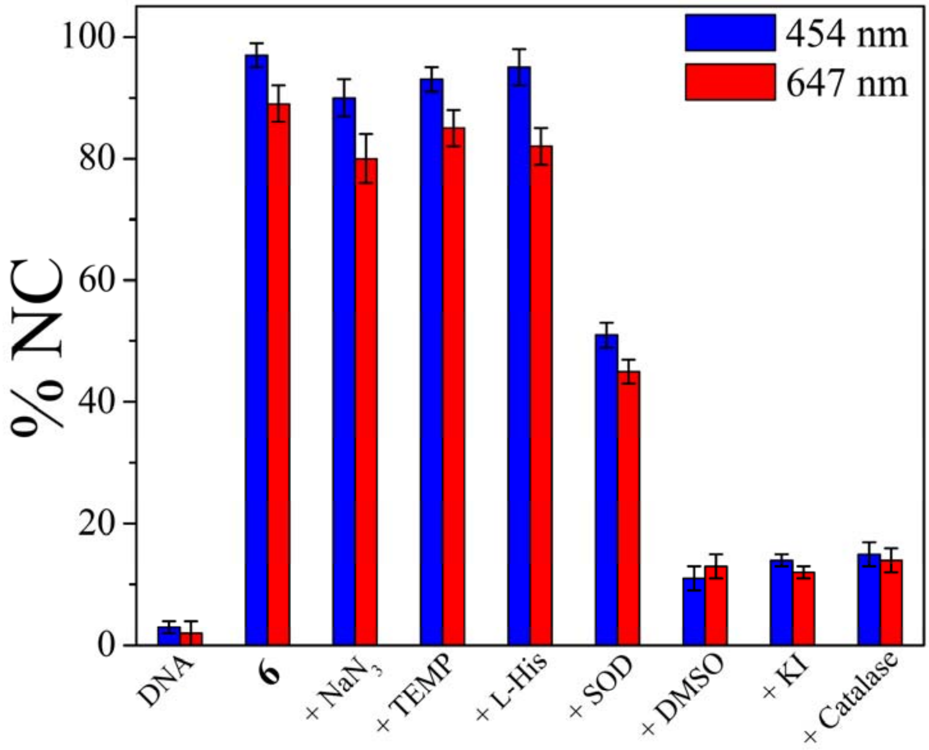

Fig. S20. Bar diagram showing the mechanistic aspects of the visible light-induced DNA cleavage activity of [Cu(Fc-Met)(pyip)](ClO_4) (**6**) at 454 nm (10 μmol) and 647 nm (15 μmol) using SC pUC19 DNA (0.2 μg, 30 μM b.p.) for an exposure time of 2 h (color code: blue, 454 nm; red, 647 nm).

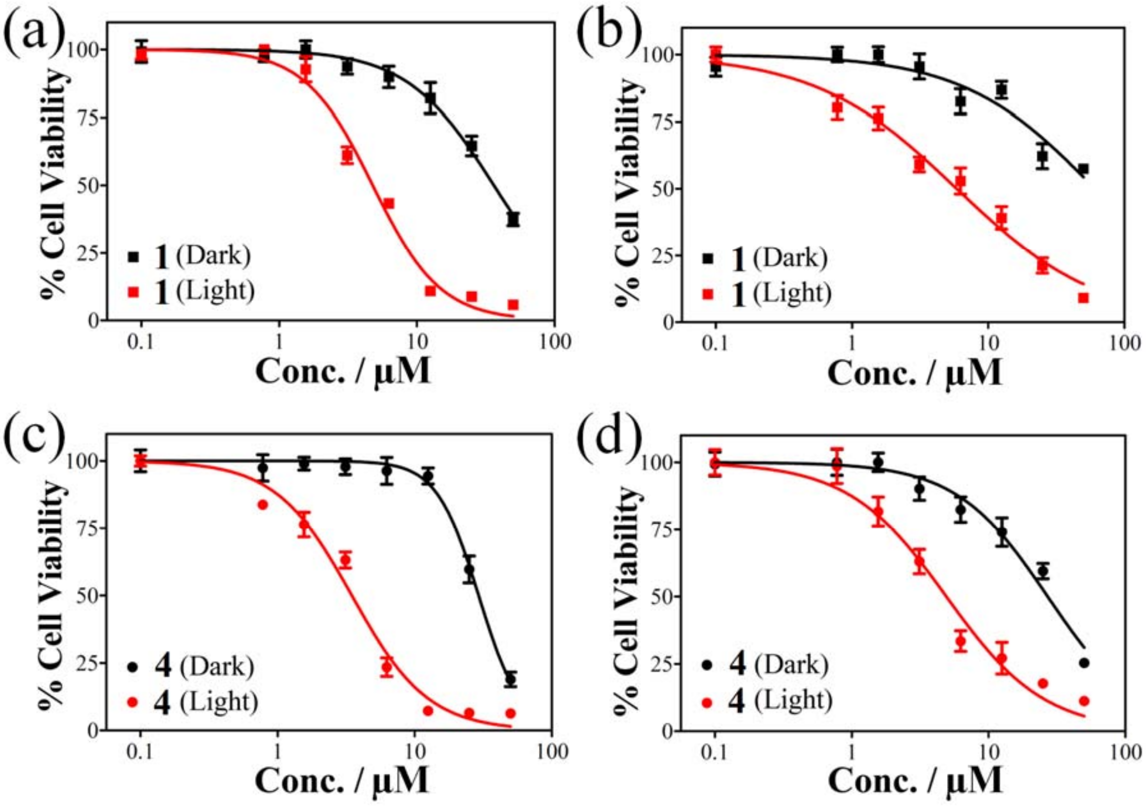

Fig. S21. Cell viability plots showing the cytotoxic effect of (a) complex **1** in HeLa cells, (b) complex **1** in MCF-7 cells, (c) complex **4** in HeLa cells and (d) complex **4** in MCF-7 cells [reaction in dark (black symbols) and in the presence of visible light of 400-700 nm (red symbols, power 10 J cm^{-2})].

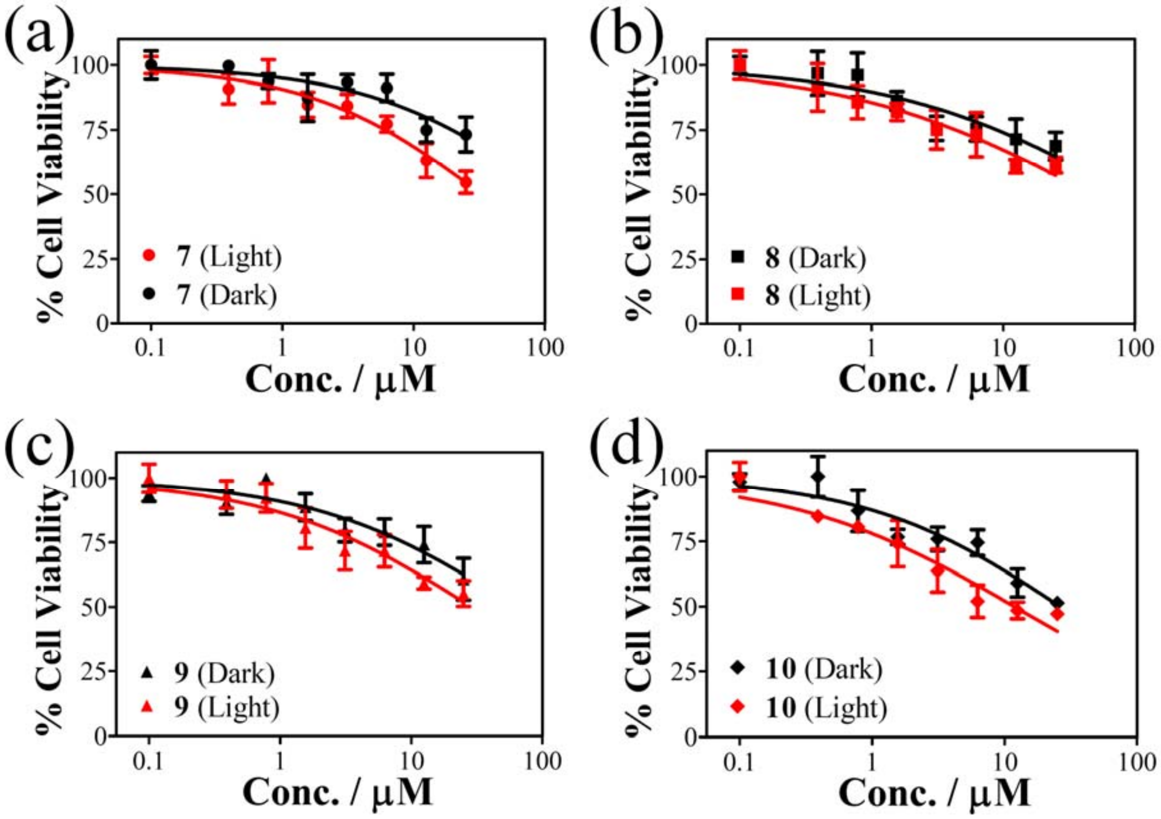

Fig. S22. Cell viability plots showing the cytotoxic effect of the complexes **7**-**10** (a-d) in HeLa cells [reaction in dark (black symbols) and in the presence of visible light of 400-700 nm (red symbols, power 10 J cm^{-2})].

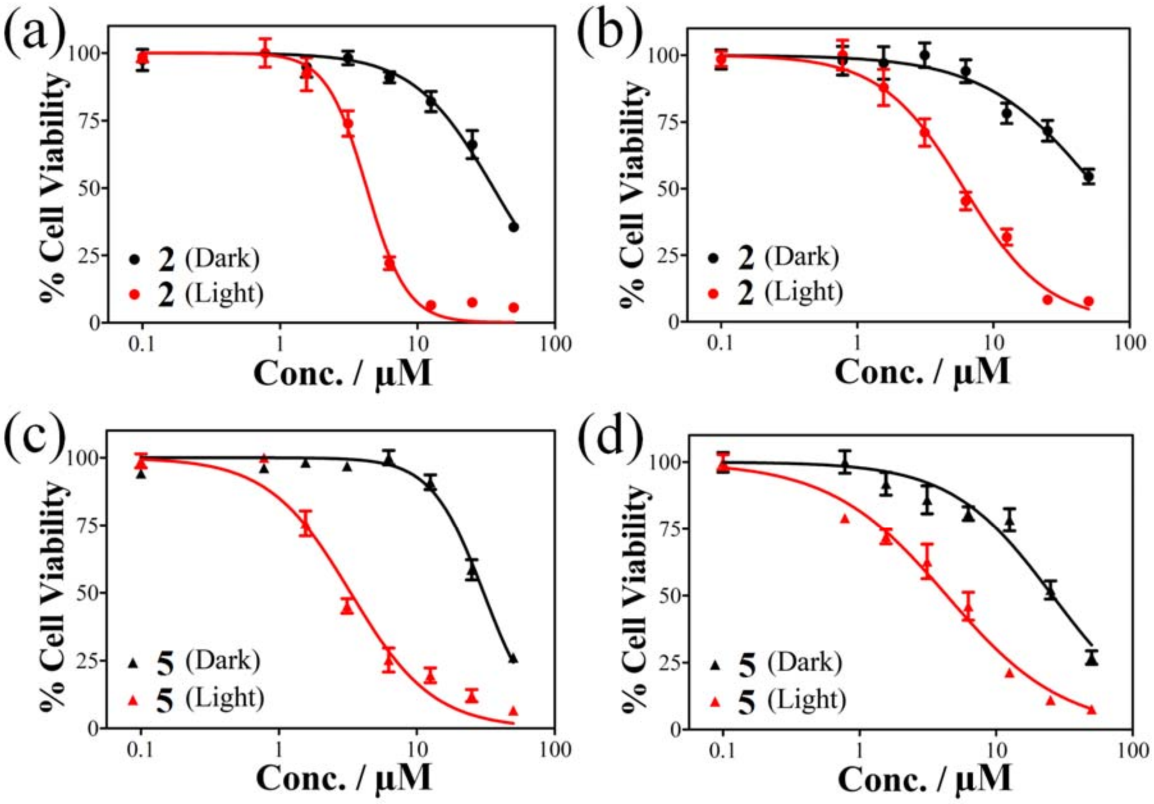

Fig. S23. Cell viability plots showing the cytotoxic effect of (a) complex **2** in HeLa cells, (b) complex **2** in MCF-7 cells, (c) complex **5** in HeLa cells and (d) complex **5** in MCF-7 cells [in dark (black symbols) and in the presence of visible light of 400-700 nm (red symbols, power 10 J cm^{-2})].

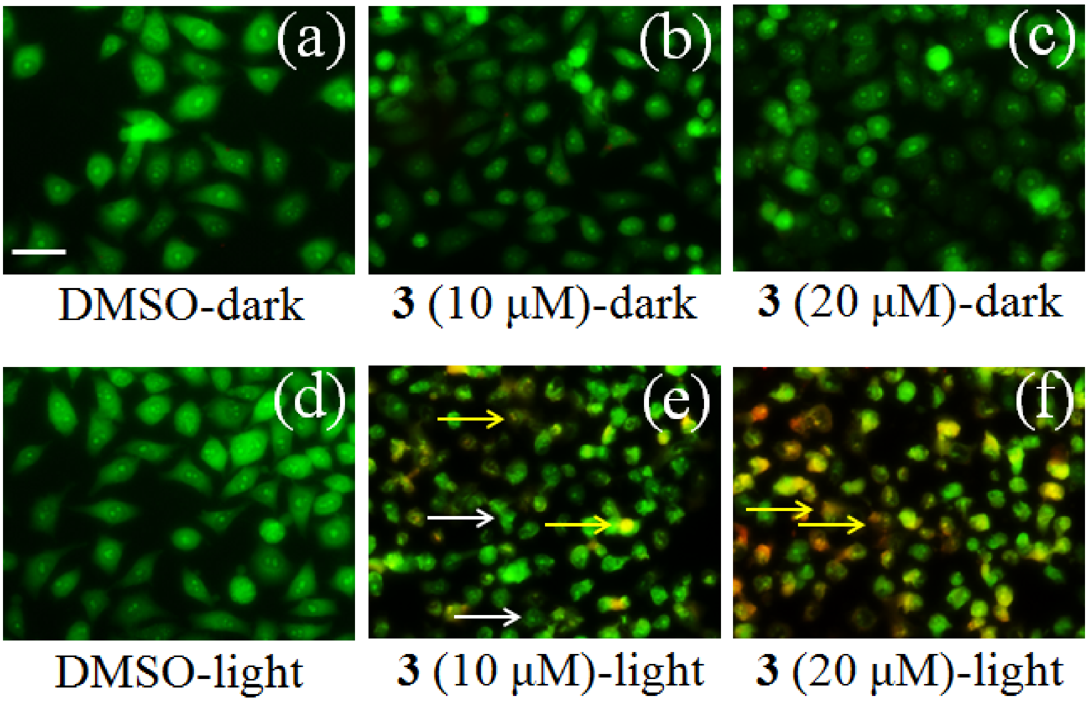

Fig. S24. Acridine orange (AO, white arrow) / ethidium bromide (EB, yellow arrow) dual staining of HeLa cells treated with complex **3** (10 and 20 μmol) to study the nuclear morphology. Panels (a) and (d) correspond to the cells treated with only DMSO in dark and light respectively, panels (b) and (c) correspond to the cells treated with complex **3** (10 and 20 μmol, respectively) in dark. Panels (e) and (f) correspond to the cells treated with complex **3** (10 and 20 μmol, respectively) and irradiated with visible light (400-700 nm, 10 J cm^{-2}). The scale bar in the panels corresponds to 20 μm.

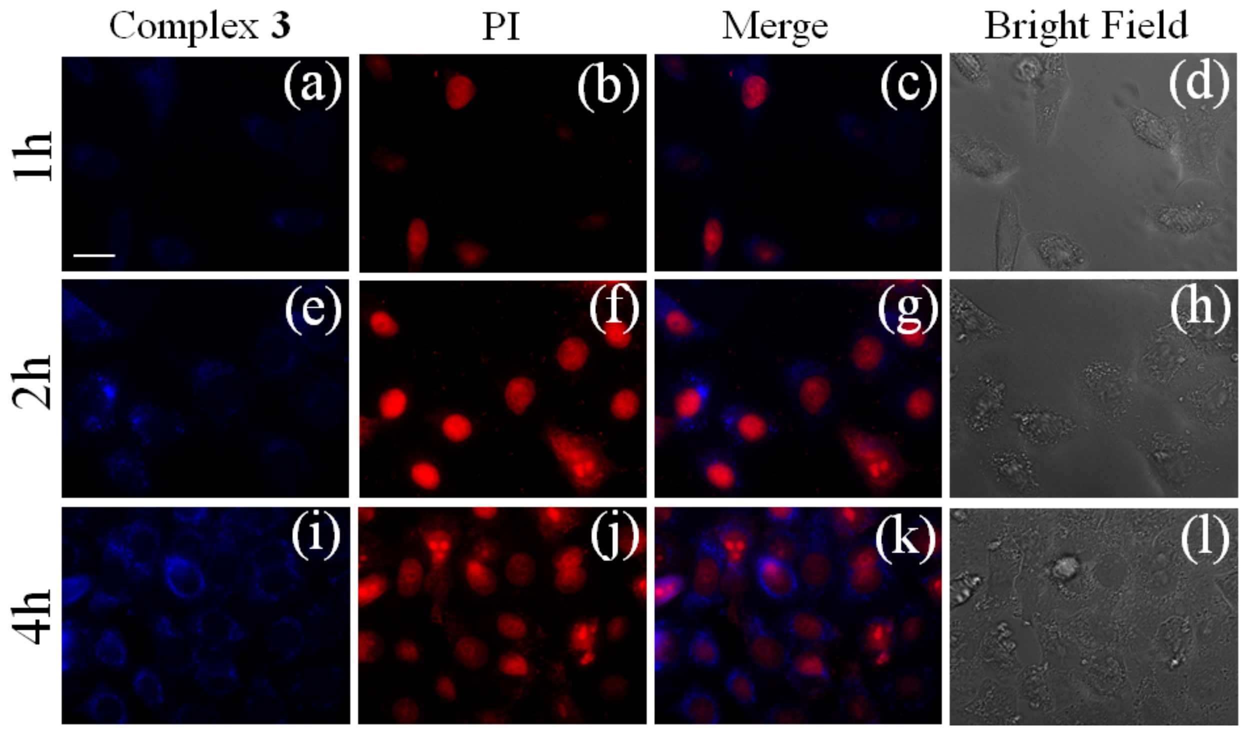

Fig. S25. A time-course collection of fluorescence microscopic images of HeLa cells treated with complex **3** (10 µmol) and propidium iodide (PI). Panels (a), (e) and (i) correspond to the blue emission of complex **3** and the respective images were taken after 1, 2 and 4 h. Panels (b), (f) and (j) correspond to the red emission of PI. Panels (c), (g) and (k) are the merged images of the first two panels. Panels (d), (h) and (l) are the bright field images. The scale bar in the panels corresponds to 20 µm.

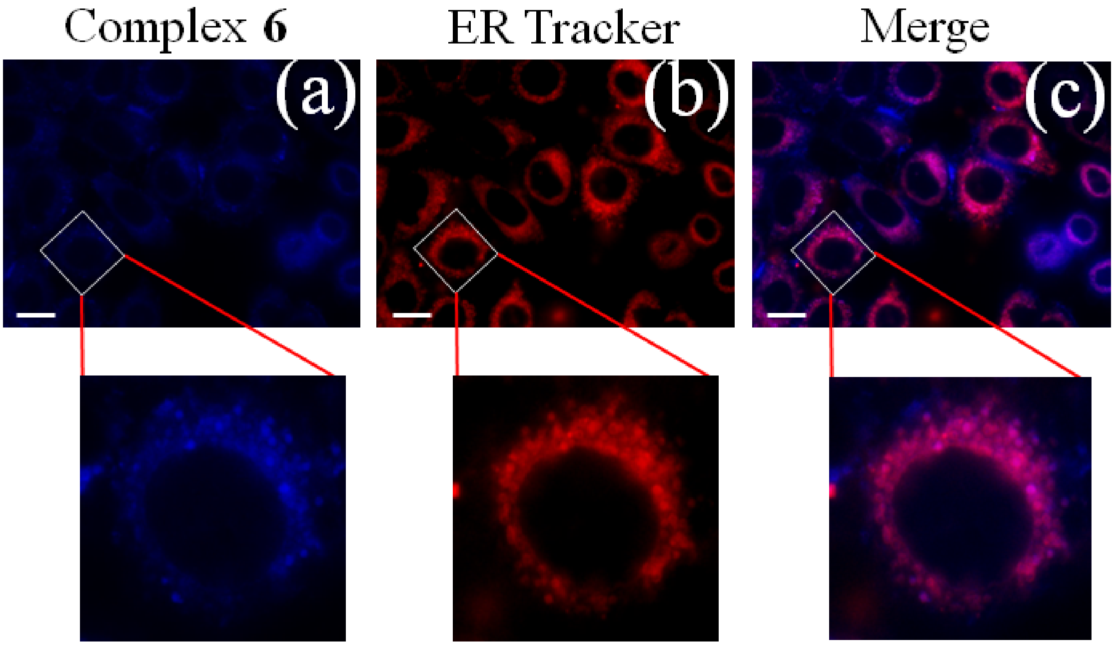

Fig. S26. Fluorescence microscopic images of HeLa cells treated with complex **6** (10 µmol) and ER Tracker Red. Panels (a), (b) and (c) correspond to the blue emission of complex **6**, red emission of ER Tracker Red and the merged images respectively **taken after 1h**. Enlarged images are shown at the bottom. The scale bar in the panels corresponds to 20 µm.

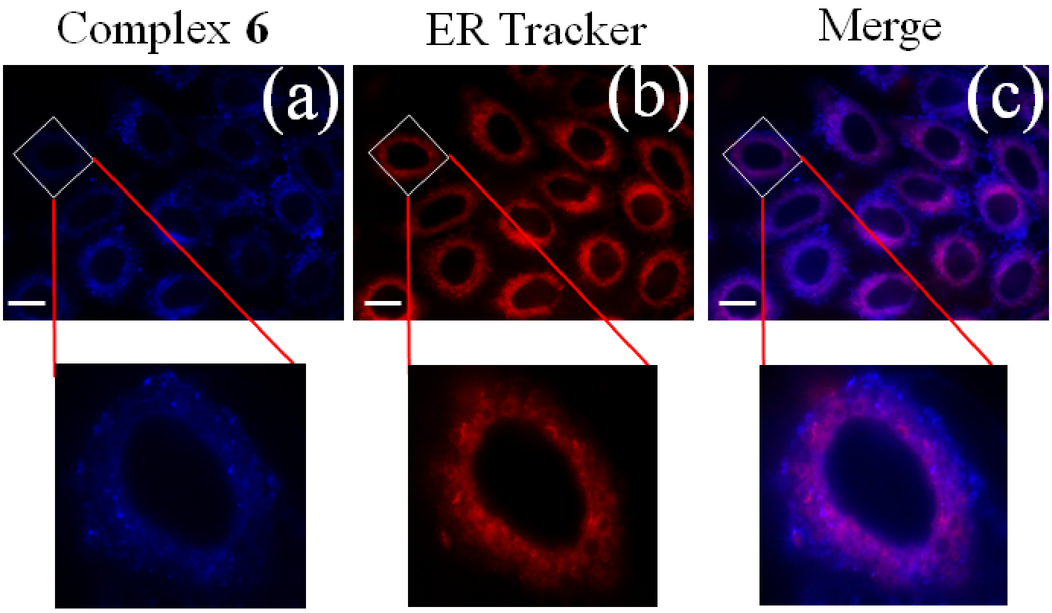

Fig. S27. Fluorescence microscopic images of HeLa cells treated with complex **6** (10 µmol) and ER Tracker Red. Panels (a), (b) and (c) correspond to the blue emission of complex **6**, red emission of ER Tracker Red and the merged images respectively **taken after 2h**. Enlarged images are shown at the bottom. The scale bar in the panels corresponds to 20 µm.

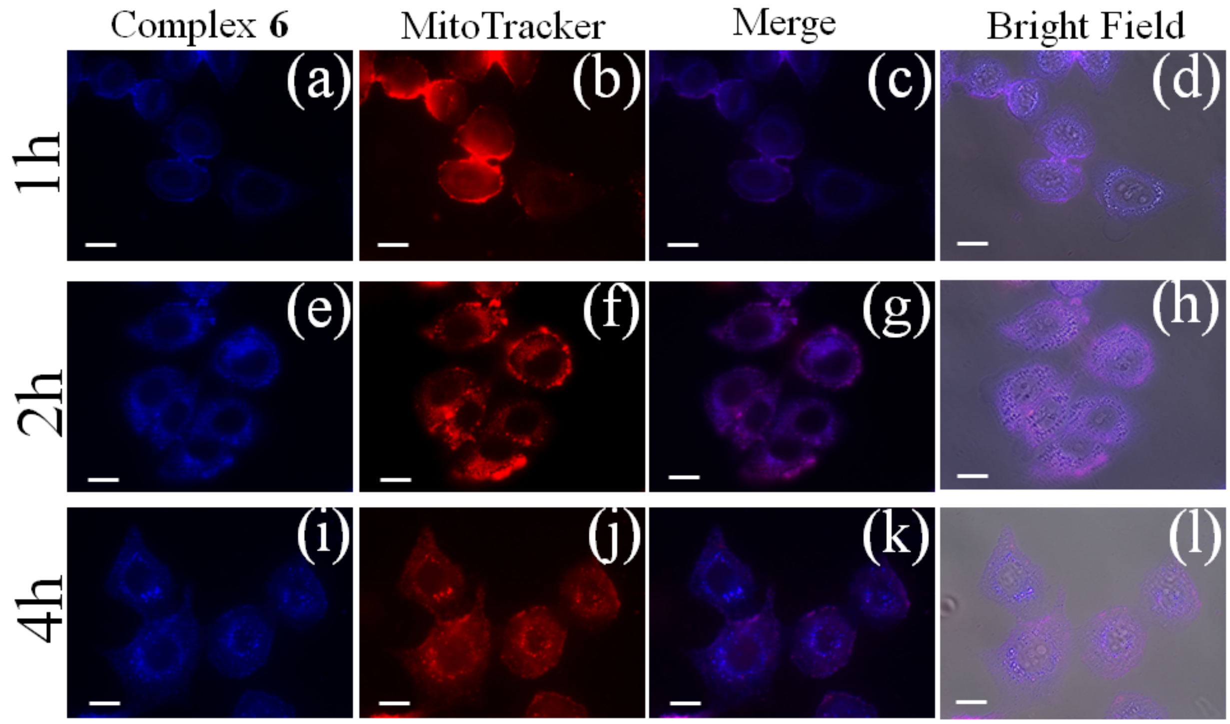

Fig. S28. A time-course collection of fluorescence microscopic images of HeLa cells treated with complex **6** (10 µmol) and MitoTracker Red. Panels (a), (e) and (i) correspond to the blue emission of complex **6** and the respective images were taken after 1, 2 and 4 h. Panels (b), (f) and (j) correspond to the red emission of MitoTracker Red. Panels (c), (g) and (k) are the merged images of the first two panels. Panels (d), (h) and (l) are the bright field images merged with the emission of complex **6** and Mito Tracker Red. The scale bar in the panels corresponds to 20 µm.

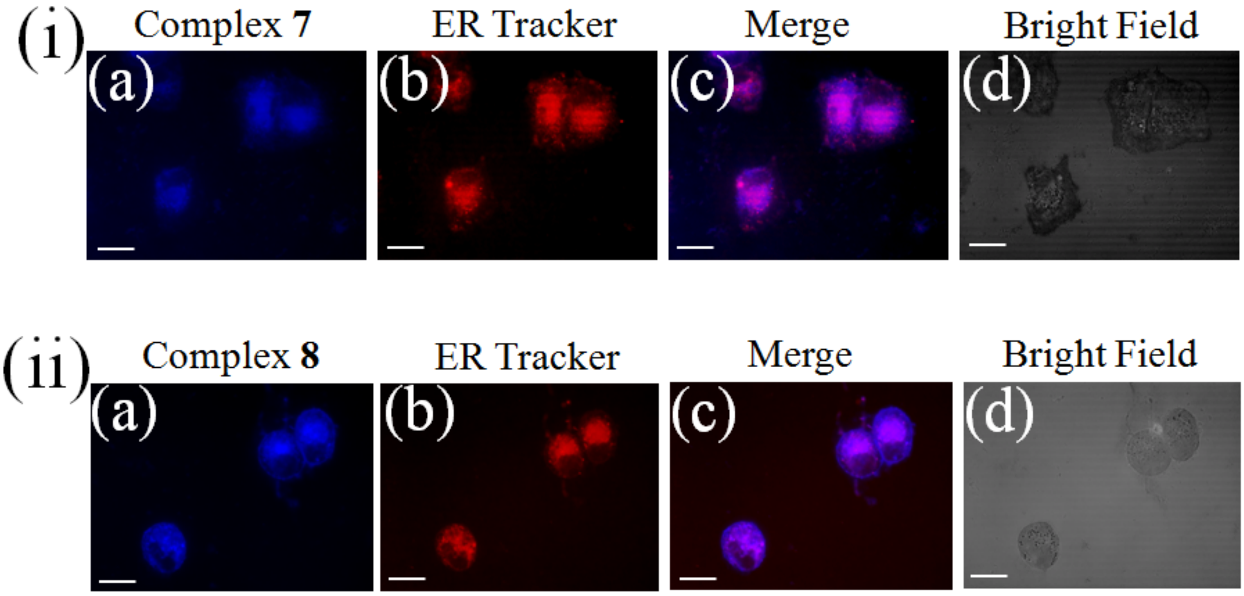

Fig. 29. Fluorescence microscopic images of HeLa cells treated with (i) complex **7** and (ii) complex **8** (10 μmol) and ER Tracker Red. Panels (a), (b), (c) and (d) correspond to the blue emission of complexes **7** or **8** taken after 2 h, red emission of ER Tracker Red, merged images of the first two panels and bright field images of the HeLa cells respectively. The scale bar in the panels corresponds to 20 μm.

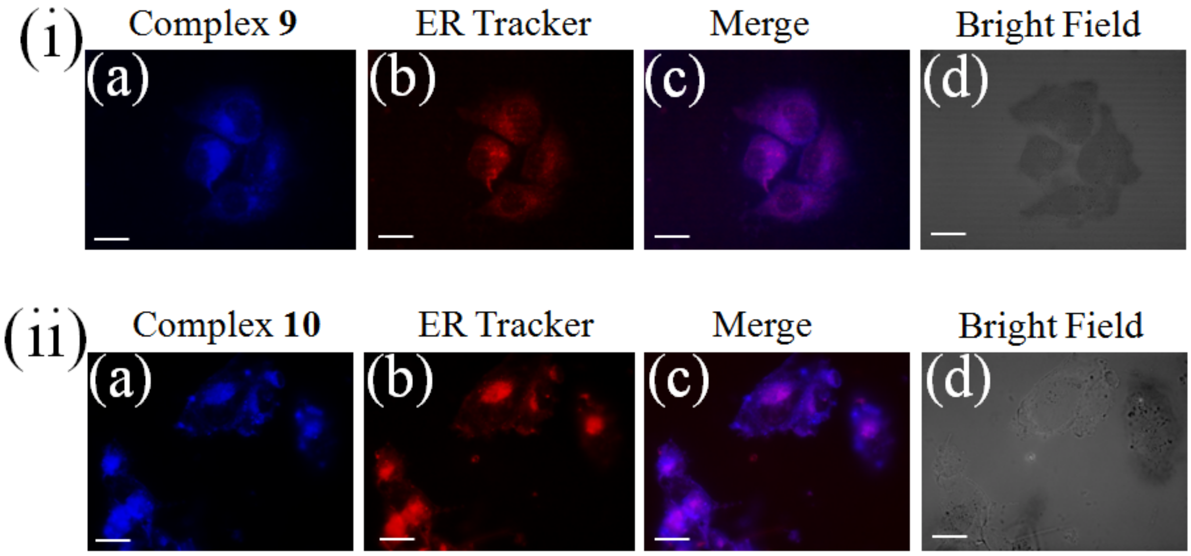

Fig. S30. Fluorescence microscopic images of HeLa cells treated with (i) complex **9** and (ii) complex **10** (10 µmol) and ER Tracker Red. Panels (a), (b), (c) and (d) correspond to the blue emission of complexes **9** or **10** taken after 2 h, red emission of ER Tracker Red, merged images of the first two panels and bright field images of the HeLa cells respectively. The scale bar in the panels corresponds to 20 µm.